

Power electronic controller with time sharing switching strategy for grid connected PV systems

Maria Jenisha CHARLES¹ , Ammasaigounden NANJAPPAGOUNDER^{1,*} ,
Binu Ben Jose DHARMAIANRETNAM² 

¹Department of Electrical and Electronics Engineering, National Institute of Technology, Tiruchirappalli,
Tamil Nadu, India

²School of Electrical Engineering, VIT University, Chennai, Tamil Nadu, India

Received: 06.04.2018

Accepted/Published Online: 28.06.2018

Final Version: 22.01.2019

Abstract: The design and implementation of a high-efficiency two-stage power electronic controller for feeding power from a photovoltaic (PV) array to the load/utility grid is proposed. The PV array is connected to the load/utility grid through a boost converter and an inverter. The boost converter is controlled by sinusoidal pulse width modulation (SPWM) pulses so as to get a clamped quasi-sinusoidal waveform at the DC link. The inverter converts the clamped quasi-DC voltage into AC voltage using the SPWM controller. At any time only one switch operates at high frequency, thus yielding reduction in the switching losses of the converters. The controller used for the inverter takes care of both the maximum power point tracking (MPPT) at unity power factor (UPF) and grid synchronization. The power electronic controller has been constructed using IGBT switches. The complete system has been modeled with MATLAB/Simulink software and simulation results are compared with experimental results. Experiments have been conducted at varying irradiances for both stand-alone (110 W) and grid-connected (110 V, 50 Hz) systems with a PV array of 130.2 V and 4.5 A employing the dSPACE DS1103 controller. The steady-state and dynamic responses of the proposed system are presented.

Key words: Grid-connected PV system, power electronic controller, SPWM switching strategy, MPPT control

1. Introduction

Renewable energy sources such as solar, wind, and biomass are widely preferred for electrical power generation due to their limitless availability and ecofriendly nature. Among such renewable energy sources, solar energy is more attractive for a country like India, which has huge potential for solar power. The application of PV offers great appeal to satisfy electricity demand in stand-alone/grid-connected power systems. A power electronic controller is employed to interface the PV source and the isolated load/grid. The simplest form of a grid-connected PV system consists of a PV array and voltage source inverter (VSI) [1–6]. The common constraint of such single-stage configurations is that the PV array voltage needs to always be higher than the peak value of the grid voltage. To overcome this limitation, an improved single-stage topology was proposed. This system would normally work with a single stage and switch to a step-up function whenever the input voltage drops below the required value. However, the inverter topology proposed has a larger number of switches, which makes the design and control complex [7, 8]. Obviously to have more flexibility, the need for two-stage conversion arises. Dastagiri et al. proposed a two-stage power conversion scheme operating with a buck converter and

*Correspondence: ammas@nitt.edu

low-frequency VSI to transfer power from a fixed DC source to a stand-alone AC load [9]. To handle a variable DC input voltage/PV source, Rong et al. and Dipankar et al. proposed a two-stage power conversion system using a high step-up converter (DC-DC) and conventional VSI [10, 11]. However the output of the VSI is used for feeding only a stand-alone AC load. Subsequently, some authors proposed two stages of power conversion using a cascaded buck-boost converter and conventional VSI for feeding the utility grid [12, 13]. In order to reduce the number of switches in the DC-DC converter of the above schemes, some authors proposed another two-stage grid integration topology with high step-up DC-DC converter and VSI [14, 15]. Due to increased switching control complexity in the above scheme, [16] proposed a two-stage power conversion with a DC-DC converter and VSI using time sharing control. In the above scheme, only one switch at any instant operates at high frequency, which makes the circuit more efficient than earlier configurations. The DC-DC converter always operates in the boost mode and the VSI inverter operates in buck mode. However, in the above scheme, a fixed DC source is considered and the output of the inverter feeds the stand-alone load.

In the present work, one such two-stage power conversion scheme is attempted with a focus on the analysis and implementation of a grid interface for a PV array, which is a variable DC source. The novelty of the work is that a modified closed-loop SPWM strategy has been developed for the integration of variable DC output PV array with stand-alone load as well as utility grid. The complexities associated with grid synchronization and simultaneously tracking maximum power in such a time sharing control are addressed in our work. The first stage is a DC-DC boost converter, which is controlled in such a way that it generates a quasi-sinusoidal waveform at the output, which will be clamped at the level of the PV array output voltage. The peak of the quasi-sinusoidal waveform is always maintained constant at the peak of the utility grid voltage, with varying irradiation. The VSI in the second stage operates in buck mode to convert the clamped quasi-sinusoidal into a symmetrical sinusoidal waveform, removing the DC offset. Furthermore, the SPWM-based controller of the VSI ensures that the maximum PV power available is supplied to the utility grid at unity power factor (UPF).

2. Proposed system

The schematic of the proposed configuration is shown in Figure 1, which consists of the PV array, boost converter, single phase H-bridge VSI, and a load/grid. The variable output of the PV array is fed as input to the boost converter. The boost converter is controlled by SPWM pulses so as to get a clamped quasi-sinusoidal wave as shown in Figure 1. The duty ratio of the boost converter is automatically adjusted in such a way that the peak of the sine portion of the output waveform is maintained at the peak value of the grid voltage. Furthermore, the DC offset value is made to follow the PV array output voltage (V_{PV}). The inverter converts this voltage at the DC bus into a symmetrical sinusoidal wave at the grid/load terminal by appropriately performing the switching operation. In the case of a grid-connected system, the inverter switching is carried out such that maximum power available in the PV array is fed to the grid at the UPF. In the proposed work, 6 PV panels of 80 W each are connected in series to achieve an array voltage (V_{oc}) of 130.2 V and array current (I_{sc}) of 4.5 A.

The PV array in the present work is modeled using a single diode model [17]. The PV cell output current (I_{PV}) and output voltage (V_{PV}) are related by Eq. (1) as follows [17]:

$$I_{PV} = I_{ph} - I_s e^{\frac{q(V_{PV} + R_s I_{PV})}{mkT}} - \frac{V_{PV} + R_s I_{PV}}{R_{sh}} \quad (1)$$

Here, I_{PV} is the PV photon current (A), I_s is the diode reverse bias saturation current (A), q is the magnitude of charge (C), k is the Boltzmann constant (J/k), T is the cell temperature (K), and R_s and R_{sh} are the

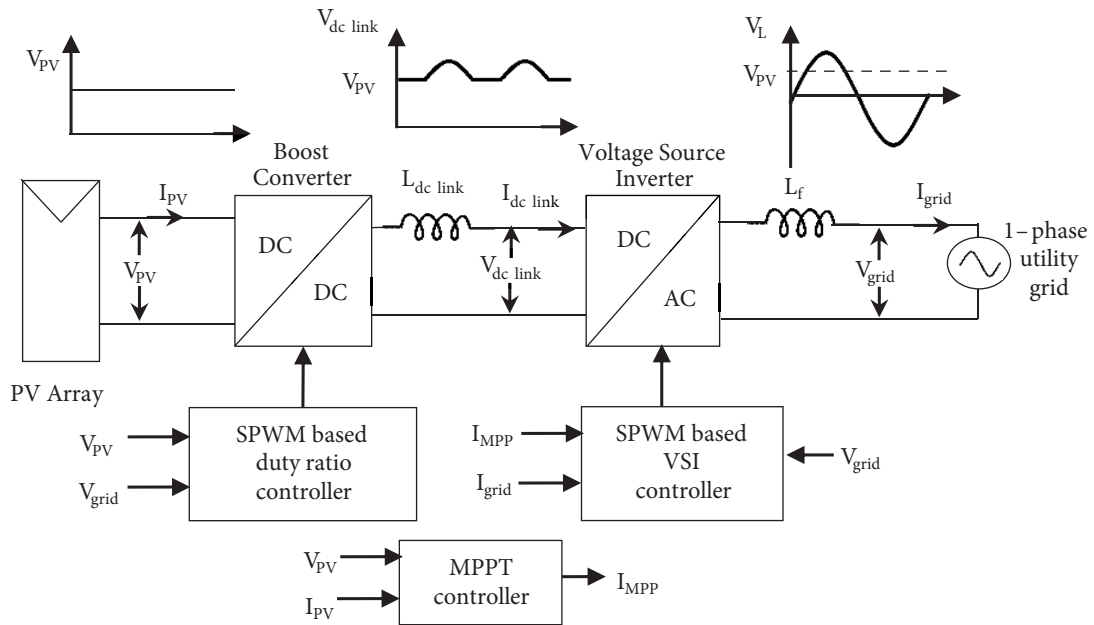


Figure 1. Block schematic of the proposed scheme.

series and shunt resistance (Ω), respectively. The experimentally obtained I-V and P-V characteristics of the constructed PV array under varying irradiation are shown in Figure 2a.

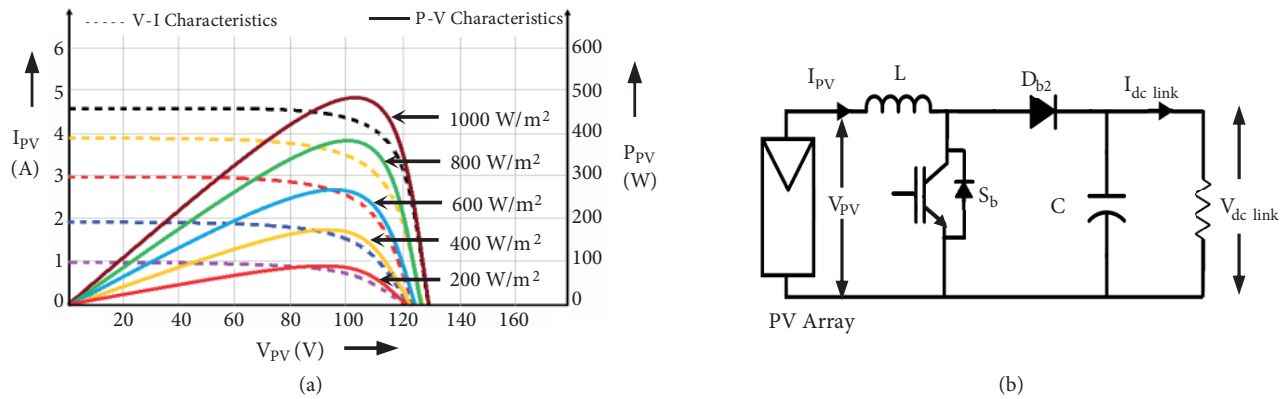


Figure 2. a) Experimentally obtained characteristics of PV array; b) schematic diagram of boost converter.

2.1. Boost converter

The proposed boost converter shown in Figure 2b uses an IGBT switch to pulse width modulate the variable DC voltage of the PV array into an inductor. The output voltage (V_{dclink}) of the boost converter, which is a clamped quasi-sine wave as shown in Figure 1, is given as

$$V_{dclink} = \frac{V_{PV}}{1 - \delta} \quad (2)$$

From Eq. (2), the duty ratio is:

$$\delta = 1 - \frac{V_{PV}}{V_{dclink}} \quad (3)$$

Since the boost converter switching is based on sinusoidal pulse width modulation (SPWM), the duty ratio is not constant for particular PV voltages. Referring to Figure 2a, the values of V_{PV} at $400 W/m^2$ (minimum irradiation) and $1000 W/m^2$ (maximum irradiation) are 96 V and 110 V, respectively. For a utility grid of 110 V, the range of duty ratio as per Eq. (3) would be as follows:

$$0 < \delta < 0.4; \quad \text{when} \left\{ \begin{array}{l} \text{irradiation} = 400 W/m^2 \\ V_{PV} = 96V \\ V_{dclink(peak)} = 155.56V \end{array} \right\} \quad (4)$$

$$0 < \delta < 0.29; \quad \text{when} \left\{ \begin{array}{l} \text{irradiation} = 1000 W/m^2 \\ V_{PV} = 110V \\ V_{dclink(peak)} = 155.56V \end{array} \right\} \quad (5)$$

The value of the inductor is selected in such a way that the ripple current is 2 times more than the minimum load current [18], as follows:

$$L = \frac{V_{dclink} - V_{PV}(1 - \delta)}{\Delta I_{dclink} f_s} \quad (6)$$

Design of the capacitor depends on the maximum allowable output voltage fluctuations [18], as given by:

$$C = \frac{I_{dclink} \delta}{\Delta V_{dclink} f_s} \quad (7)$$

Here, ΔI_{dclink} is the ripple in current, ΔV_{dclink} is the ripple voltage, f_s is the switching frequency (Hz), and I_{dclink} is the current at the DC link (A). Based on Eqs. (6) and (7), the critical values of the inductor and capacitor are obtained as 0.538 mH and 1.12 μ F, respectively, for $V_{PV} = 96 V$, $V_{dclink(peak)} = 155.56 V$, $\delta = 0.4$, and $f_s = 20 kHz$. To make the converter operate in continuous conduction mode, the inductor and capacitor values are chosen to be larger than the critical values. The values of various parameters used in the boost converter circuit are furnished in Table 1.

Table 1. Values of parameters used in the boost converter.

Parameter	Value
Inductor, L	2 mH
Capacitor, C	10 μ F/250V
Input DC voltage, V_{PV}	96–110 V
Output voltage, V_{dclink}	$V_{PV} - 155.56 V$

3. Working principle of the proposed scheme

The power circuit of the proposed scheme, which consists of a PV array, inductors L and L_{dclink} , capacitor C, diodes D_{b1} and D_{b2} , and five IGBT switches (S_b, S_1, S_2, S_3, S_4) along with a filter circuit, is shown in Figure 3a. The boost converter is switched such that its output, which is the DC link voltage, is a clamped quasi-sinusoidal waveform. The buck operation is carried out by the inverter at required instants to shape the DC link voltage into a symmetrical sinusoidal voltage at the load terminal.

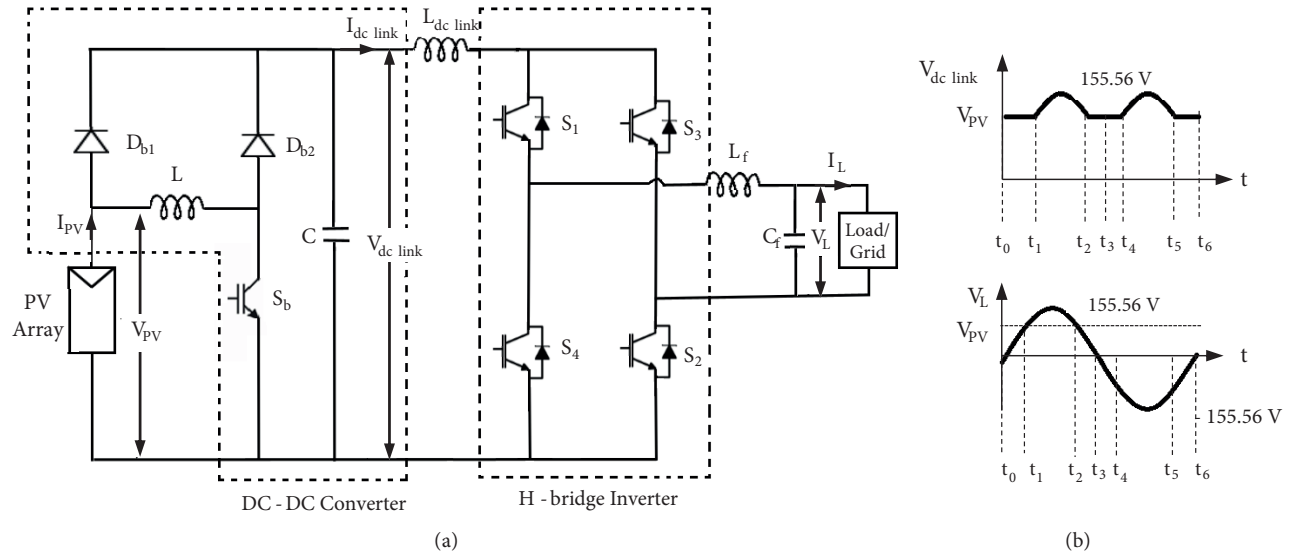


Figure 3. a) Power circuit of the proposed scheme; b) voltage waveforms at the DC link and inverter output during one cycle of time sharing operation.

3.1. Time sharing operation of the proposed scheme

The time sharing operation of the proposed scheme is explained using the waveforms at the output of boost converter (V_{dclink}) and VSI (V_L) as shown in Figure 3b.

From t_0 to t_1 and t_2 to t_3 : During this period, the output voltage (V_L) required is less than the input voltage (V_{PV}). Hence, the H-bridge inverter is operated as a buck converter with S_1 operating at high-frequency switching modulation and S_2 being in continuous ‘on’ position. During this period S_3, S_4 switches are off, diode D_{b1} is on, and D_{b2} is off as it is a reverse biased condition.

From t_1 to t_2 : During this period, the output voltage (V_L) required is greater than the input voltage (V_{PV}), so the DC-DC converter is operated in boost mode by switching S_b at high-frequency switching modulation with S_1 and S_2 switches in the ‘on’ position; diode D_{b1} is off as it is reverse biased, D_{b2} is on, and S_3, S_4 are in the ‘off’ position. The positive half cycle of the output is obtained.

From t_3 to t_4 and t_5 to t_6 : During this period, the output voltage (V_L) has to be less than the input voltage (V_{PV}). Hence, the H-bridge inverter is operated as a buck converter. S_3 is operating at high-frequency switching modulation with S_4 in ‘on’ position. S_b, S_1, S_2 switches are off, diode D_{b1} is on, and D_{b2} is off.

From t_4 to t_5 : During this period, the output voltage (V_L) has to be greater than input voltage (V_{PV}). Hence, to operate the converter in boost mode S_b is switching at high frequency with S_3 and S_4 switches on. D_{b1} is off as it is reverse biased, D_{b2} is on, and S_1, S_2 are open. The negative half cycle of the output is obtained. The diode D_{b1} will act as a bypass diode when V_{PV} is greater than the instantaneous value of V . During this time, the proposed configuration will operate as single-stage PV grid-connected system, resulting in reduced power losses.

The switching sequence of the devices for the above time sharing operation is given in Table 2. It can be noted that only one switch in a full cycle will be operating at high frequency. On the other hand, in conventional two-stage topology, the switch in the boost converter will work with the high-frequency PWM switching and the switches in the H-bridge inverter will work with high-frequency SPWM switching. Hence, the proposed

Table 2. Switching sequence for time sharing operation of the proposed scheme.

Time period	Requirement	Switching status		Output of VSI
t_0 to t_1 and t_2 to t_3	$V_L < V_{PV}$	ON	$S_{1(HF)}, S_2, D_{b1}$	Positive half cycle
		OFF	S_b, S_3, S_4, D_{b2}	
t_1 to t_2	$V_L > V_{PV}$	ON	$S_{b(HF)}, S_1, S_2, D_{b2}$	
		OFF	D_{b1}, S_3, S_4	
t_3 to t_4 and t_5 to t_6	$V_L < V_{PV}$	ON	$S_{3(HF)}, S_4, D_{b1}$	Negative half cycle
		OFF	S_b, S_1, S_2, D_{b2}	
t_4 to t_5	$V_L > V_{PV}$	ON	$S_{b(HF)}, S_3, S_4, D_{b2}$	
		OFF	D_{b1}, S_1, S_2	

time sharing switching scheme will result in reduced converter switching and conduction losses. As the inverter generates a proper sine wave at the output, the rating of the filter required is less compared to the conventional two-stage topology.

3.2. SPWM-based duty ratio controller

Figure 4a shows the switching technique for the SPWM-based boost converter to generate a clamped quasi-sinusoidal waveform at the output.

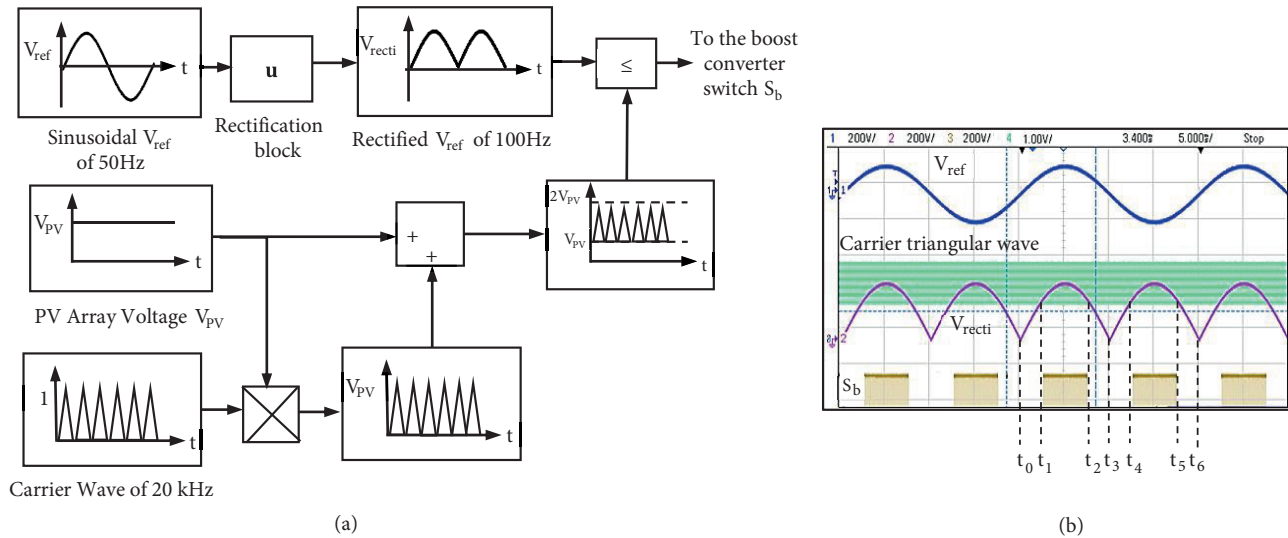


Figure 4. a) Switching technique for SPWM-based duty ratio controller; b) switching pulses experimentally obtained for boost converter from dSPACE controller.

Here the carrier signal is a triangular wave of frequency 20 kHz, which is multiplied by V_{PV} . The output signal from the multiplier is added again with V_{PV} and then compared with the rectified sinusoidal voltage (V_{recti}) signal of 100 Hz, having a peak value of 155.56 V corresponding to the proposed utility grid voltage of 110 V. The pulses generated from the comparator are given to the boost switch. The converter performs a

quasi-sinusoidal boost operation (V_{PV} to $V_{ref(peak)}$) at the DC link. For an isolated system, the reference sine wave is generated internally as per the required load voltage and for a grid-connected system the voltage at the grid terminal is sensed and given as input to the rectification block.

The switching pulses obtained using this control technique for the boost converter employing the dSPACE controller are shown in Figure 4b. When the irradiation is low, the output voltage at the PV array (V_{PV}) will be reduced. Correspondingly, the amplitude of the carrier wave is reduced, which increases the high-frequency operating period (t_1 to t_2 and t_4 to t_5) of the boost converter. On the other hand, when the irradiation is high, the high-frequency operating period of the boost converter will be reduced.

3.3. SPWM-based VSI controller

3.3.1. Stand-alone load

The H-bridge inverter consists of four IGBT switches, S_1 to S_4 . The upper switches in both legs S_1 and S_3 are controlled by SPWM pulses. Here the carrier signal is a triangular wave of frequency 20 kHz multiplied by V_{PV} , compared against the reference modulating signal, which is a quasi-sinusoidal voltage of frequency 100 Hz with peak magnitude of 155.56 V. The switches in lower legs S_2 and S_4 of the H-bridge inverter are controlled by continuous 50 Hz square pulses of duty ratio 50% as shown in Figure 5a. The experimentally generated switching pulses for the inverter from the dSPACE controller are shown in Figure 5b.

When the irradiation is low, the output voltage at the PV array (V_{PV}) will be reduced. Correspondingly, the amplitude of the carrier wave is reduced, which increases the high-frequency operating period (t_1 to t_2 and t_4 to t_5) of the boost converter. The high-frequency operating period (t_0 to t_1 , t_2 to t_4 , and t_5 to t_6) of the inverter will be reduced accordingly. On the other hand, when the irradiation is high, the operating period of the boost converter will be reduced and the high-frequency operating period of the inverter will be increased. It is to be noted that the modulating signal, PV voltage, and carrier wave for the VSI controller are the same as those of the duty ratio controller. For the sake of clarity, the control scheme of the VSI is shown separately in Figure 5a.

3.3.2. Grid-connected system

In the grid-connected system, IGBT switches S_1 to S_4 of the inverter are being controlled by SPWM pulses to pump the maximum power to the grid. For achieving MPPT control and grid synchronization, the voltage at the grid terminal is sensed and given to the phase-locked loop (PLL) block as shown in Figure 6, which produces a saw-tooth waveform of grid frequency. This output of the PLL is given to a sine block to generate a sine wave of unity magnitude at grid frequency. The MPP current (I_{MPP}) from the MPPT controller is multiplied by the unity magnitude sine wave to generate the sine current reference ($I_{grid(ref)}$) for the inverter switching. The $I_{grid(ref)}$ is compared with the actual grid current (I_{grid}) and the error signal is given to the PI controller to produce the error-corrected signal. The output of the PI controller is compared against a triangular carrier wave of 20 kHz and the generated SPWM pulses are given to the inverter switches, as shown in Figure 6. The VSI will operate in high frequency from the time range t_0 to t_6 , in order to incorporate grid synchronization along with MPPT at the inverter. This control technique ensures that the available PV power is supplied to the utility grid with UPF.

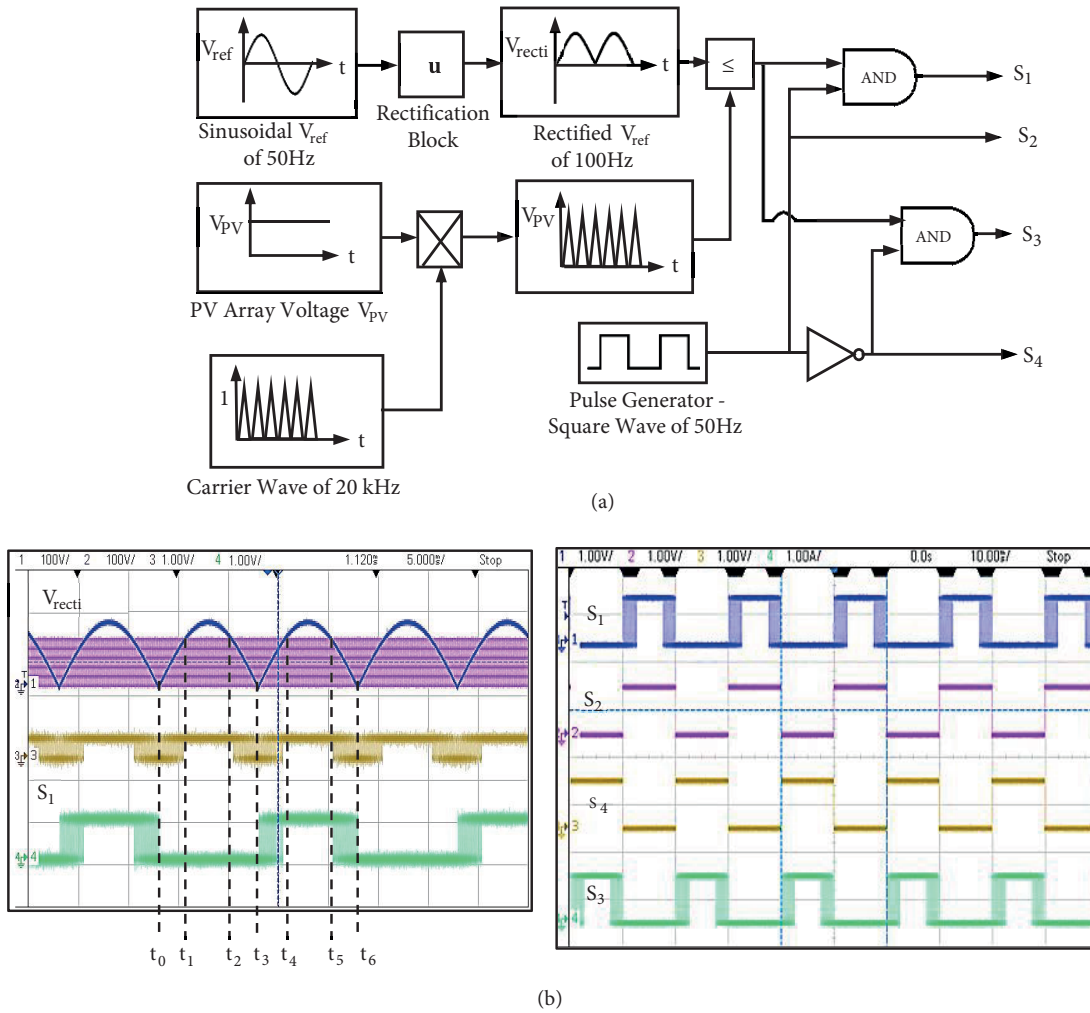


Figure 5. a) Switching technique for SPWM-based VSI controller; b) experimentally generated gate pulses for VSI using dSPACE controller.

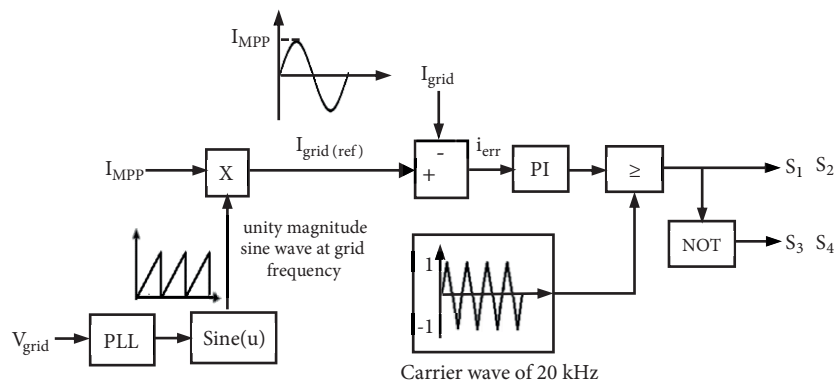


Figure 6. Switching technique for grid-connected VSI controller.

3.3.3. MPPT controller

The MPPT block tracks the maximum power of the PV array using a simple perturb & observe (P&O) method by sensing the voltage (V_{PV}) and current (I_{PV}) of the PV array. The power output (P_{PV}) of the PV array is calculated from the measured values of V_{PV} and I_{PV} . The maximum power point current at the k th instant is:

$$I_{MPP}(k) = I_{MPP}(k-1) + \Delta i; \quad \left\{ \begin{array}{l} P_{PV}(k) > P_{PV}(k-1) \text{ and } V_{PV}(k) > V_{PV}(k-1) \text{ or} \\ P_{PV}(k) < P_{PV}(k-1) \text{ and } V_{PV}(k) < V_{PV}(k-1) \end{array} \right\} \quad (8)$$

$$I_{MPP}(k) = I_{MPP}(k-1) - \Delta i; \quad \left\{ \begin{array}{l} P_{PV}(k) < P_{PV}(k-1) \text{ and } V_{PV}(k) > V_{PV}(k-1) \text{ or} \\ P_{PV}(k) > P_{PV}(k-1) \text{ and } V_{PV}(k) < V_{PV}(k-1) \end{array} \right\} \quad (9)$$

The output of the MPPT controller (I_{MPP}) is given to the VSI controller for appropriate switching of the inverter to pump maximum power to the grid. The power output of PV array is:

$$P_{PV} = V_{PV} * I_{PV} \quad (10)$$

The power fed to the grid is:

$$P_{grid} = V_{grid} I_{grid} \cos \phi \quad (11)$$

Since power fed to the grid terminal is at UPF, $\phi = 0^\circ$.

Hence,

$$P_{grid} = V_{grid} * I_{grid} \quad (12)$$

$$P_{grid} = \frac{V_{grid} I_{MPP}}{\sqrt{2}} \quad (13)$$

Assuming $P_{PV} = P_{grid}$ for MPPT, $V_{grid} * I_{grid} = \frac{V_{grid} * I_{MPP}}{\sqrt{2}}$,

$$I_{MPP} = \frac{\sqrt{2} V_{PV} I_{PV}}{V_{grid}} \quad (14)$$

For example, referring to Figure 2a, at an irradiation of 1000 W/m^2 , the maximum power output of the PV array is 456 W. To pump this maximum power to the grid, the IMPP from the MPPT controller is 5.86 A, as per Eq. (14). The corresponding current at the grid terminal for the maximum power is 4.15 A.

4. Simulation and experimental results of the proposed system

To validate the effective operation of the proposed system, a simulation study has been carried out using the simpower systems toolbox in MATLAB software for both stand-alone and grid-connected cases. The PV array is modeled using a single diode equivalent circuit [16]. The power from the PV source is transported to the AC load/grid through a boost converter and VSI. Both the DC-DC converter and VSI are modeled using the components available in MATLAB/Simulink. The boost converter parameters given in Table 1 along with $L_f = 10 \text{ mH}$ and $C_f = 22 \mu\text{F}$ are chosen for the simulation study. In order to suppress the inrush current of the capacitor at the DC link, a small value of L_{dlink} (20 mH) is selected for both simulation and experimentation.

A resistive load of 110 W at the AC side is considered for the stand-alone system and a utility grid of 110 V and 50 Hz is considered for the grid-connected system.

For experimentation, six 80 W panels are connected in series, which have V_{oc} of 21.7 V and I_{sc} of 4.5 A each under standard test conditions. An IGBT (CT60AM - 600 V, 40 A)-based conventional boost converter with bypass diode and a single phase H-bridge (SKM150IGB12T4 - 1200 V, 150 A) VSI are used. Two control techniques are employed in the proposed system: one for the boost converter to produce a clamped quasi-sine wave at the DC link and another for the inverter to make the clamped quasi-sine wave input into symmetrical sine wave output, both switching techniques being implemented using the dSPACE DS1103 controller. The dSPACE controller is a hardware interface that can generate DSP codes for MATLAB models. It consists of analog to digital (ADC) and digital to analog (DAC) converters and an RS232 serial interface. It downloads the codes to the controller board for executing the program in real time. Hence, this controller helps in generating required gate pulses for the power electronic converters based on the external inputs from the sensors.

Voltages (V_{PV} and V_{grid}) and currents (I_{PV} and I_{grid}) are sensed through external voltage (LV25-P) and current transducers (LA55-P), respectively, and the outputs of the sensors are fed to the ADC with appropriate scaling factor. The pulses for the control of the boost converter and VSI are produced as explained in Section 3.2 and Section 3.3. The gate pulses obtained would be available at the DAC output. The gate pulse for the boost converter is passed through a high frequency opto-coupler (HCPL) circuit, which produces isolation as well as signal conditioning before being fed to the IGBT. The gate pulses for VSI are passed through ULN2003 op-amp circuits for signal conditioning and then to gate drivers to operate the IGBT switches in the inverter. The experiment was conducted for different irradiations to analyze the performance of the proposed scheme for both isolated and grid-connected cases.

4.1. Results with stand-alone load

The steady-state response of the stand-alone system for irradiation of 1000 W/m^2 is shown in Figure 7. At the irradiation of 1000 W/m^2 , the voltage produced at the PV array output terminal is 110 V, and to satisfy the AC load, the average value of DC current drawn from the PV array, which is also flowing through the boost inductor, is 1.19 A. These waveforms are shown in Figure 7a. Figure 7b shows the clamped quasi-sine wave at the DC link, which has peak voltage of 155.56 V and average current of 0.85 A. The AC load of 110 W is satisfied by consuming the voltage of 110 V and current of 1 A as shown in Figure 7c. Fast Fourier transform (FFT) analysis has been carried out for the proposed control scheme and the AC voltage harmonics are observed to be 0.8%.

The dynamic response of the stand-alone system when the irradiation changes from 1000 W/m^2 to 600 W/m^2 is shown in Figure 7d. The switching strategy of the boost converter is such that the peak DC link voltage always remains at 155.56 V. Hence, it meets the load demand irrespective of the change in PV irradiation as shown in Figure 7d.

4.2. Results with utility grid

For the grid-connected system, at an irradiation of 1000 W/m^2 , the maximum power at the PV array is 456 W, as shown in Figure 2a. The maximum voltage and current at the PV array are 110 V and 4.15 A, respectively. Figure 8a shows the clamped quasi-sine wave at the DC link, which has a peak voltage of 155.56 V and an average current of 3.8 A. To pump this maximum power to the grid, the MPPT controller generates I_{MPP} of

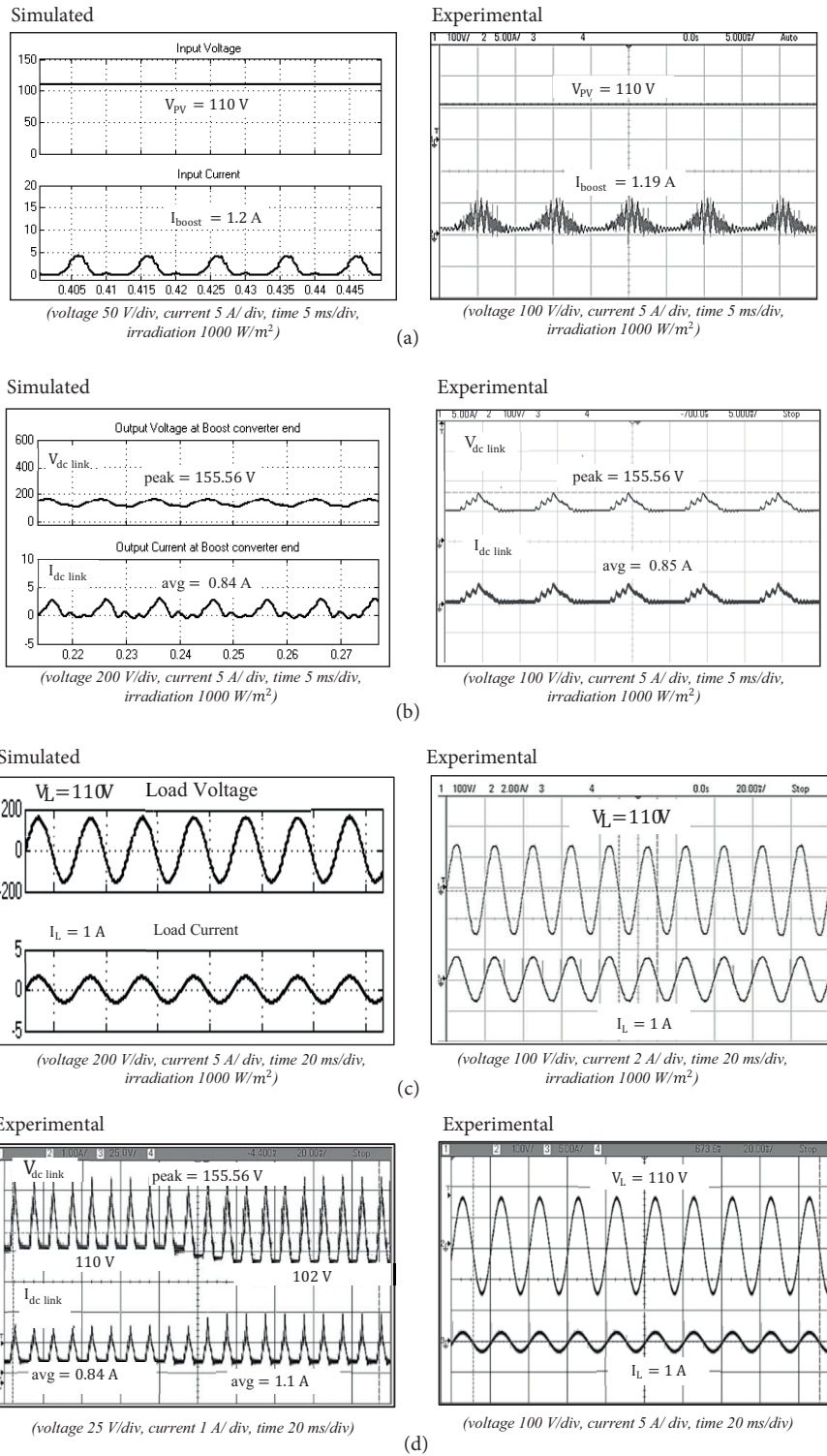


Figure 7. Voltage and current waveforms with stand-alone load: a) at the input of boost converter, b) at the DC link, c) at the load terminals, d) response of the system at DC link and at load terminals when irradiation changes from 1000 W/m² to 600 W/m².

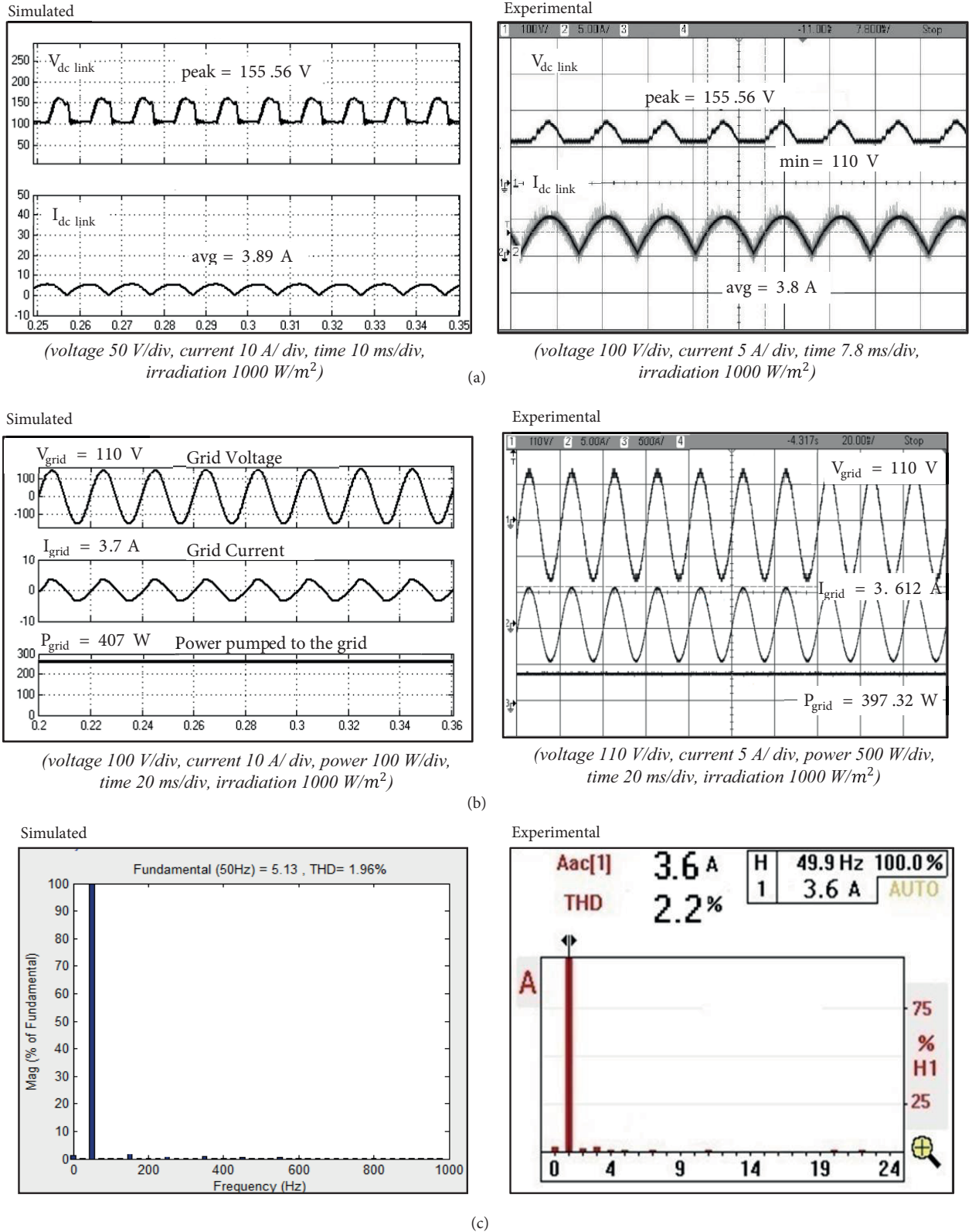


Figure 8. a) Voltage and current waveforms at the DC link, b) voltage and current waveforms at the grid terminals, c) grid current THD.

5.1 A. The VSI controller in turn produces pulses to the inverter to pump this power to the grid at UPF, as explained. The voltage and current at the grid terminal for the irradiation of 1000 W/m^2 are 110 V and 3.612 A , respectively, as shown in Figure 8b. It is to be mentioned here that the I_{MPP} and I_{grid} values at this irradiation of 1000 W/m^2 have been reported as 5.86 A and 4.15 A , respectively. The minor deviation from these values in the practical situation is attributed to the losses in the converters. Figure 8c shows the total harmonic distortion (THD) of the grid current, which is well within the IEEE 519 standards [19].

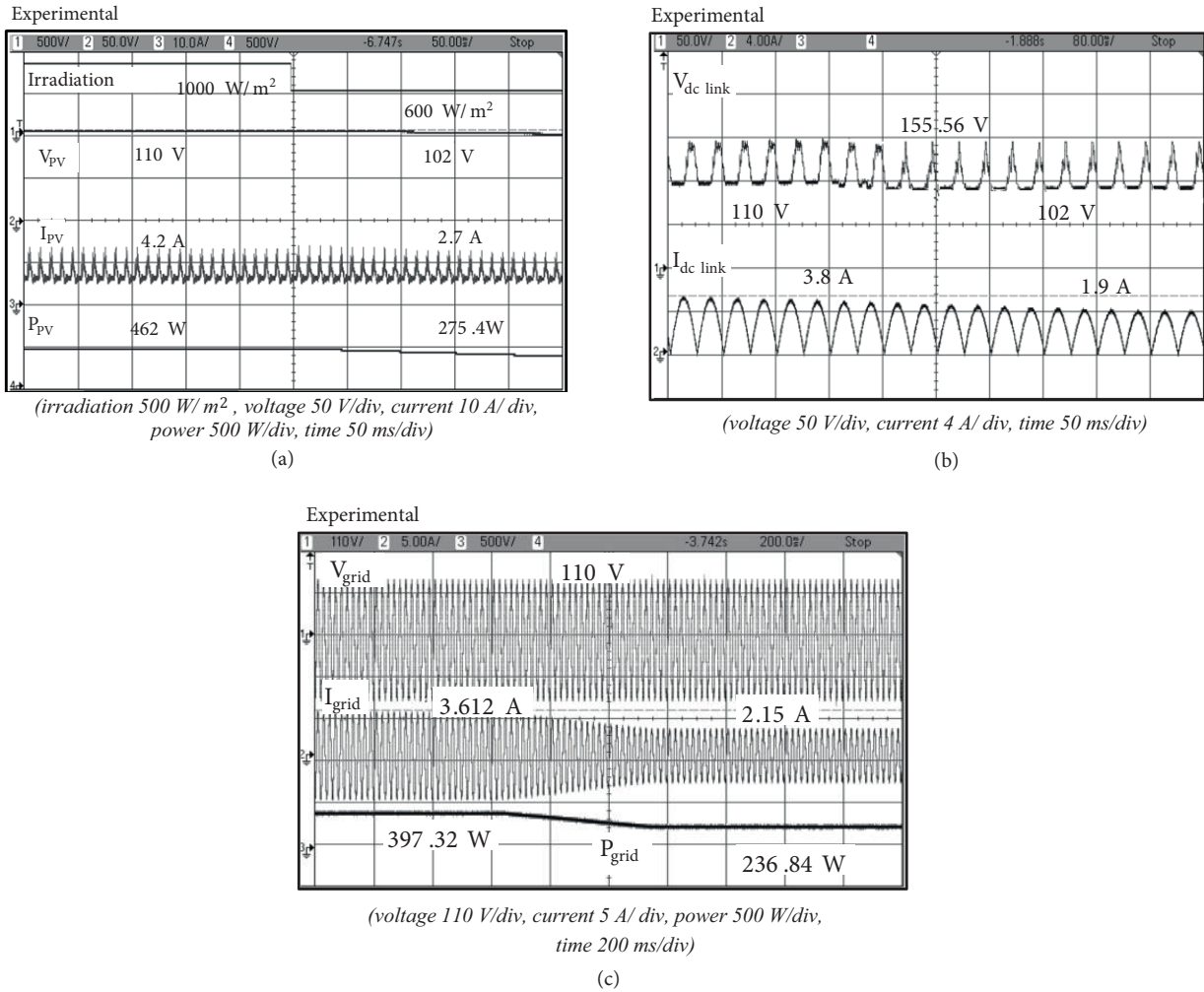


Figure 9. Experimentally obtained voltage and current waveforms when irradiation changes from 1000 W/m^2 to 600 W/m^2 : a) at the PV array, b) at the DC link, c) at the grid terminals.

The proposed switching strategy is also tested for dynamic change in irradiation. With the change in irradiation from 1000 W/m^2 to 600 W/m^2 , the PV voltage correspondingly changes from 110 V to 102 V as shown in Figure 9a. The switching strategy of the boost converter is such that the peak of DC link voltage remains at the $V_{grid(peak)}$, which is 155.56 V as shown in Figure 9b. Hence, to feed this maximum power to the grid, the MPP current (I_{MPP}) changes from 5.1 A to 3 A , the grid current changes from 3.612 A to 2.15 A , and the power changes from 397.32 W to 236.84 W at the grid terminal, as shown in Figure 9c. The photograph of the experimental setup of the proposed system is shown in Figure 10.

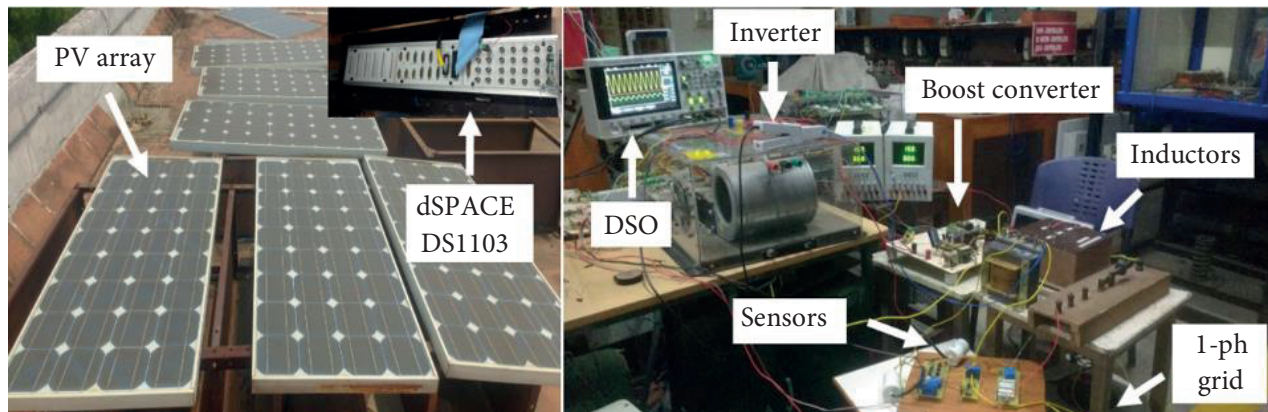


Figure 10. Photograph of the experimental setup of the proposed system.

5. Conclusion

An efficient control scheme has been implemented for a PV system with an integrated two-stage power converter (boost converter and VSI) for feeding power to the load/grid. The SPWM switching employed for the boost converter generates a clamped quasi-sinusoidal waveform at the DC link, which is converted to a pure sine wave by the VSI with a smaller filter. This output of the inverter is synchronized with the utility grid of 110 V and 50 Hz, using a PLL circuit. The inverter switching is controlled in such a way that the maximum power available at the PV array output is fed to the grid at unity power factor. For this, a grid current reference is generated by sensing the grid voltage. The efficiencies of the boost converter and VSI are 96% and 91%, respectively, yielding an overall efficiency of 87%. Furthermore, it is optimistically envisaged that more reduction in losses will occur if the IGBT switches are operated at their specified rating, while in the present case they have been utilized far below their maximum rating. For comparison, the proposed topology was tested with conventional switching operation and it was observed that the overall efficiency was about 10% less than that of the time sharing operation. The simplicity of the controller has also been demonstrated with a stand-alone load as well, for which the reference sine wave is generated internally as per the required load voltage. The SPWM control logic for both the boost converter and for the inverter is implemented using a dSPACE DS1103 controller. The experimental results of the proposed system at various stages are presented and are compared with the simulation results for both steady-state and dynamic conditions. The test results demonstrate that the proposed scheme can be effectively employed in small-scale solar PV systems feeding microgrids.

References

- [1] Chen Y, Smedley KM. A cost-effective single-stage inverter with maximum power point tracking. *IEEE T Power Electr* 2004; 19: 1289-1294.
- [2] Jain S, Agarwal V. A single-stage grid connected inverter topology for solar PV systems with maximum power point tracking. *IEEE T Power Electr* 2007; 22: 1928-1940.
- [3] Gonzalez R, Gubia E, Lopez J, Marroyo L. Transformerless single-phase multilevel-based photovoltaic inverter. *IEEE T Ind Electron* 2008; 55: 2694-2702.
- [4] Araujo SV, Zacharias P, Mallwitz R. Highly efficient single-phase transformerless inverters for grid-connected photovoltaic systems. *IEEE T Ind Electron* 2010; 57: 3118-3128.

- [5] Xiao H, Xie S, Chen Y, Huang R. An optimized transformerless photovoltaic grid-connected inverter. *IEEE T Ind Electron* 2011; 58: 1887-1895.
- [6] Sreekanth T, Lakshminarasamma N, Mishra MK. A single-stage grid-connected high gain buck-boost inverter with maximum power point tracking. *IEEE T Energy Conver* 2017; 32: 330-339.
- [7] Hantschel J. Direct current-voltage converting method for use in inverter involves clocking switch units such that high potential and input direct current voltage lie at inputs of storage reactor in magnetized and free wheel phases respectively. German Patent DE102006010694 A1, 2007.
- [8] Sasidharan N, Singh JG. A novel single-stage single-phase reconfigurable inverter topology for a solar powered hybrid AC/DC home. *IEEE T Ind Electron* 2017; 64: 2820-2828.
- [9] Reddy BD, Selvan MP, Moorthi S. Simplified embedded control scheme for two-stage multistring off-grid inverter. *IET Power Electron* 2014; 7: 2954-2963.
- [10] Wai RJ, Wang WH, Lin CY. High-performance stand-alone photovoltaic generation system. *IEEE T Ind Electron* 2008; 55: 240-250.
- [11] Debnath D, Chatterjee K. Two-stage solar photovoltaic-based stand-alone scheme having battery as energy storage element for rural deployment. *IEEE T Ind Electron* 2015; 62: 4148-4157.
- [12] Ho BMT, Chung HSH. An integrated inverter with maximum power tracking for grid-connected PV systems. *IEEE T Power Electr* 2005; 20: 953-962.
- [13] Zhao Z, Xu M, Chen Q, Lai JS, Cho Y. Derivation, analysis, and implementation of a boost-buck converter-based high-efficiency PV inverter. *IEEE T Power Electr* 2012; 27: 1304-1313.
- [14] Jiang S, Cao D, Li Y, Peng FZ. Grid-connected boost-half-bridge photovoltaic microinverter system using repetitive current control and maximum power point tracking. *IEEE T Power Electr* 2012; 27: 4711-4722.
- [15] Evran F. Plug-in repetitive control of single-phase grid-connected inverter for AC module applications. *IET Power Electron* 2017; 10: 47-58.
- [16] Ahmed NA, Lee HW, Nakaoka M. Dual-mode time-sharing sinewave-modulation soft switching boost full-bridge one-stage power conditioner without electrolytic capacitor DC link. *IEEE T Ind Appl* 2007; 43: 805-813.
- [17] Daniel SA, Ammasai Gounden N. A novel hybrid isolated generating system based on PV fed inverter-assisted wind-driven induction Generators. *IEEE T Energy Conver* 2004; 19: 416-422.
- [18] Muhammad HR. *Power Electronics - Circuits, Devices, And Applications*. 3rd ed. Noida, India: Pearson, 2011.
- [19] IEEE. *Std 519-2014 (Revision of IEEE Std 519-1992) - IEEE Recommended Practice and Requirements for Harmonic Control in Electric Power Systems*. New York, NY, USA: IEEE, 2014.